

Contents lists available at ScienceDirect

Petroleum Science

journal homepage: www.keaipublishing.com/en/journals/petroleum-science



Original Paper

Towards in-depth profile control using s-MPG synergy with MSRG in fractured-vuggy carbonate reservoirs



Wei-Peng Wu ^a, Min Yang ^a, Dong-Chen Ma ^a, Ji-Rui Hou ^b, Tuo Liang ^{c,*}, Ming Qu ^d, Tao Tan ^a, Biao Yang ^a, Guo-Rui Ma ^a

- a Sinopec Key Laboratory of Enhanced Oil Recovery in Fractured-Vuggy Reservoirs, Sinopec Northwest Oilfield Company, Urumqi, 830014, Xinjiang, China
- ^b Unconventional Petroleum Research Institute, China University of Petroleum (Beijing), Beijing, 102249, China
- ^c Xi'an Shiyou University, Xi'an, 710065, Shaanxi, China
- ^d Sanya Offshore Oil and Gas Research Institute, Northeast Petroleum University, Sanya, 572025, Hainan, China

ARTICLE INFO

Article history: Received 30 April 2024 Received in revised form 13 September 2024 Accepted 19 September 2024 Available online 21 September 2024

Edited by Yan-Hua Sun

Keywords: Fractured-vuggy reservoir High temperature High salinity Anti-dilution s-MPG synergy with MSRG

ABSTRACT

In-depth profile control is a crucial technique employed to enhance oil recovery in fractured-vuggy carbonate reservoirs. However, it is a challenge to achieve in-depth profile control. In this paper, two types of organic gel systems, namely s-MPG and MSRG, tailored for fractured-vuggy reservoirs with $140~^{\circ}$ C and 22×10^4 mg/L have been developed. FTIR was used to analyze the functional groups of s-MPG and MSRG. Additionally, the quality retention rates of s-MPG and MSRG were assessed using TG-DSC, yielding results of 92.85% and 92.65%, respectively. The dilution rates of s-MPG and MSRG are found to be 18.69% and 26.69%, respectively, demonstrating excellent compatibility and adaptability. The enhancement performance depends on the synergistic effect that the anti-dilution s-MPG effectively separates bottom water, while high-strength MSRG separates the oil layer. Moreover, the EOR performances of s-MPG synergy with MSRG in various types of fractured-vuggy carbonate models were also evaluated. The highest oil recovery of 12% is achieved in fracture network model. Laboratory results indicate that the synergistic combination of s-MPG and MSRG for water plugging in fractured-vuggy carbonate reservoirs results in a more effective enhancement of oil recovery compared to using a single gel system for plugging. Finally, the s-MPG synergy with MSRG has been applied in actual fracturedvuggy carbonate reservoirs. As expected, the water cut of typical well is reduced from 100% to 30% and the increased oil production is 1142 t totally. Therefore, this study presents a novel approach to achieving in-depth profile control by leveraging the synergistic effect of s-MPG with MSRG in fractured-vuggy carbonate reservoirs.

© 2024 The Authors. Publishing services by Elsevier B.V. on behalf of KeAi Communications Co. Ltd. This is an open access article under the CC BY-NC-ND license (http://creativecommons.org/licenses/by-nc-nd/4.0/).

1. Introduction

Carbonate reservoir is an important oil and gas resource. At present, proven oil and gas reserves account for 60% of the total oil and gas resources in the word, which plays an important role in increasing reserves and production of oil and gas reservoir resources (Li et al., 2023; Wen et al., 2023). Tahe Oilfield is the first 100 million tons Paleozoic marine large oil field in China. Due to the combined effects of structural deformation and rock mass dissolution, the reservoir space is mainly developed in the form of

High molecular weight polymer gel is one of the main technical method for profile control and water plugging (Wu et al., 2022a).

solution cave, fracture, and dissolution cavity, showing large scale difference and significant heterogeneity (Wang et al., 2022a). The average burial depth of the reservoir ranges from 5000 to 7000 m. Besides, the salinity of formation water is generally more than 20×10^4 mg/L and the content of calcium and magnesium ions is more than 1.0×10^4 mg/L (Jiao, 2019; Wu et al., 2022b). After years of water flooding and high-energy edge and bottom water influx, the reservoir appears serious dominant channel, resulting in a large amount of remaining oil which cannot be effectively mobilized. Therefore, water control in fractured-vuggy reservoir is more complicated than that in sandstone reservoir (Qu et al., 2018; Zhao et al., 2020).

^{*} Corresponding author. E-mail address: 2262452605@qq.com (T. Liang).

Due to the high temperature and high salinity, many types of gel systems have been facing serious problems such as dilution and structural degradation, resulting in the gel losing its function in the reservoir (Emad et al., 2021). Research indicates that most chemical agents rely on van der Waals forces or hydrogen bonds to enable the intersection and association of molecular chains, thereby forming a 3D network structure (Parikh et al., 2023). The 3D network structure can endure prolonged immersion in the water phase without immediate dissolution. The identical electric charges between molecular chains repel each other, which facilitates the formation of more irregular network structures. Therefore, the gel can dissolve in water phase to form a non-Newtonian fluid with a specific breakthrough pressure gradient (Jothi Arunachalam and Saravanan, 2023).

In order to restrain the rise of water cut, plenty of profile control agents have also been developed in recent years. Wu et al. (2022a) developed an anti-high-temperature and high-salinity polymer gel that can maintain a dehydration rate of only 5% over a period of 30 days. Salunkhe et al. (2021) developed a kind of HT-PPG which can withstand temperature of 150 °C for over 18 months. Khoshkar et al. (2020) found that the nano-PPG can not only increase the sweep efficiency of water flooding bus also improve the oil production in low salinity water reservoirs. Lu et al. (2024) prepared a novel modified nano-graphite hybrid polymer gel which is capable of resisting temperatures up to a maximum of 154.9 °C. The nanographite hybrid polymer gel exhibited remarkable bound water contents as high as 21.14%. Du et al. (2023) found that the effects and abilities of in-depth profile control can be further strengthened by using dispersed particle gels (DPG) particles. Most gel systems are evaluated only by cores plugging tests. However, there is a lack of evaluation method related to dynamic plugging of gel system in fractured-vuggy carbonate reservoirs. In addition, plenty of field pilot tests show that the practical application effect of single gel in fractured-vuggy carbonate reservoir is not ideal. Therefore, it is necessary to further optimize the physicochemical properties of the gel plugging agent on the basis of the previous research, and put forward a method of synergistic application of the two plugging agents.

In this manuscript, the self-healing multi-polymer gel (s-MPG) and modified starch resin gel (MSRG) are prepared using aqueous solution polymerization method. The prepared gels can adapt to 140 °C and 22 \times 10⁴ mg/L brine solution. The concentration of hightemperature stabilizer cobalt chloride hexahydrate (CCH) used in the preparing s-MPG is very low. Thus, the high-temperature stabilizer can cause negligible damage to the formation. Besides, polymers can degrade spontaneously in long-term high temperature environments and the aqueous solution of phenolic crosslinker was also neutralized (Dong et al., 2023; Wu et al., 2022a). The amide group existing in MSRG can degrade with thermal oxidation after a period time at high temperature. Therefore, the intermolecular activity for both s-MPG and MSRG can gradually decrease with the time during application in-situ, and eventually liquid will be formed after complete failure (Wang et al., 2022b; Xu et al., 2024).

In this work, the synergistic mechanisms of s-MPG and MSRG for in-depth profile control in fractured-vuggy carbonate reservoirs are proposed. FTIR and TG-DSC method are carried out to analyze the gel structures, mass change, and thermal stability. The anti-dilution properties of s-MPG and MSRG are also evaluated. The several typical structural models of fractured-vuggy reservoirs are designed and manufactured to reveal the EOR mechanisms and effects. Eventually, the pilot test in the Tahe Oilfield is conducted to confirm the abilities of s-MPG and MSRG in-depth profile control.

2. Experimental

2.1. Preparation of self-healing multi-polymer gel and modified starch resin gel

Self-healing multi-polymer gel (s-MPG) is prepared using polymer AP-1 (AM-co-AMPS, provided by SNF Co., Ltd., China), water soluble phenolic resin crosslinker HP-JL, thiourea stabilizer

Table 1 AFW components for experiment.

Ingredients, mg/L							Total salinity, mg/L
Na ₂ SO ₄	NaHCO ₃	NaBr	NaI	NaCl	$MgCl_2$	CaCl ₂	
234.375	49.923	231.75	11.7	201940.4	9598.95	36281.19	238348.3

Table 2 Similarity criterion (Yang and Zhang, 2022).

Similar condition	Similarity formula	Physical meaning	Similarity coefficient
Geometric similarity	$\pi_1 = d/l$	Ratio of vuggy diameter	1
	$\pi_2 = B/1$	Ratio of aperture	1
Dynamic similarity	$F_{\rm G} = \Delta P(\rho_0 g d)$	Ratio of injection pressure to gravity	1.01-1.04
	$Re = \rho u l / \mu$	Ratio of inertia force to viscous force	1
Kinematic similarity	$F_{\rm O} = Q/(r^2u)$	Ratio of liquid production to injection	1.01-1.04
Similarity of characteristic parameters	$\pi_2 = \xi$	Coordination number	1
	$\pi_3 = \eta$	Filling degree	1

Table 3Design of physical simulation parameters based on similarity criterion.

	Vuggy diameter <i>d</i> , cm	Pressure <i>P</i> , kPa	Viscosity μ , mPa·s	Density ρ , g/cm ³	Acceleration g, m/s ²	Velocity Q, m ³ / h	Aperture <i>B</i> , mm	Coordination number
Reservoir	500-2500	≈ 45000	≈100	0.87-0.92	9.8	1-1.5	0.5-5	3-20
Physical model	0.5-16	1000	70-80	0.81-0.85	9.8	0.0003-0.0006	1-3	3-20
Similarity coefficient	166.67-200.00	45	1.25	1.07	1	2500-3333	1.67-2.00	1

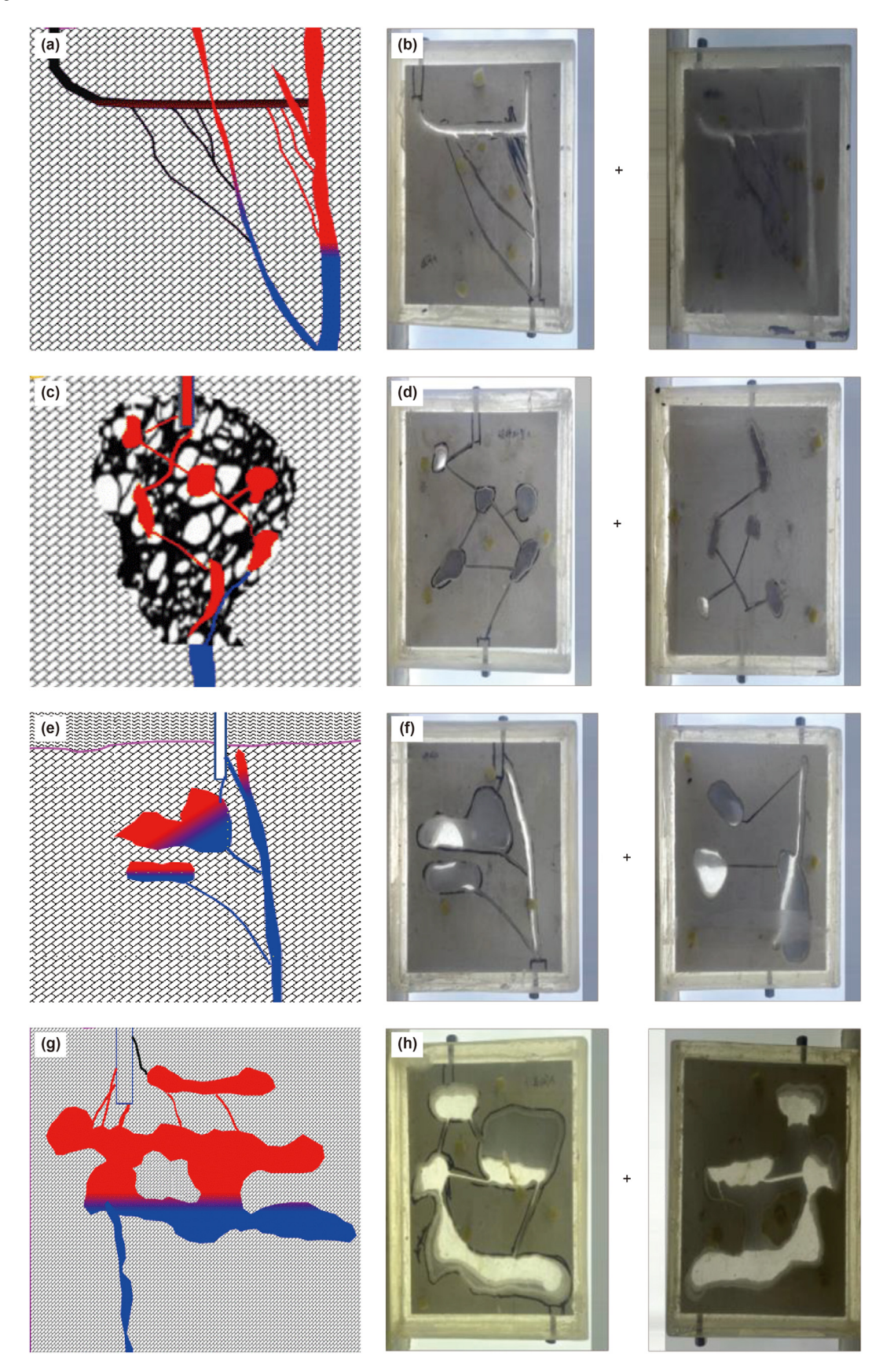


Fig. 1. Physical simulation models of different types. Theoretical and physical models of fracture network (a, b), fragmentation zone (c, d), fractured-vuggy (e, f), and karst-cave (g, h), respectively.

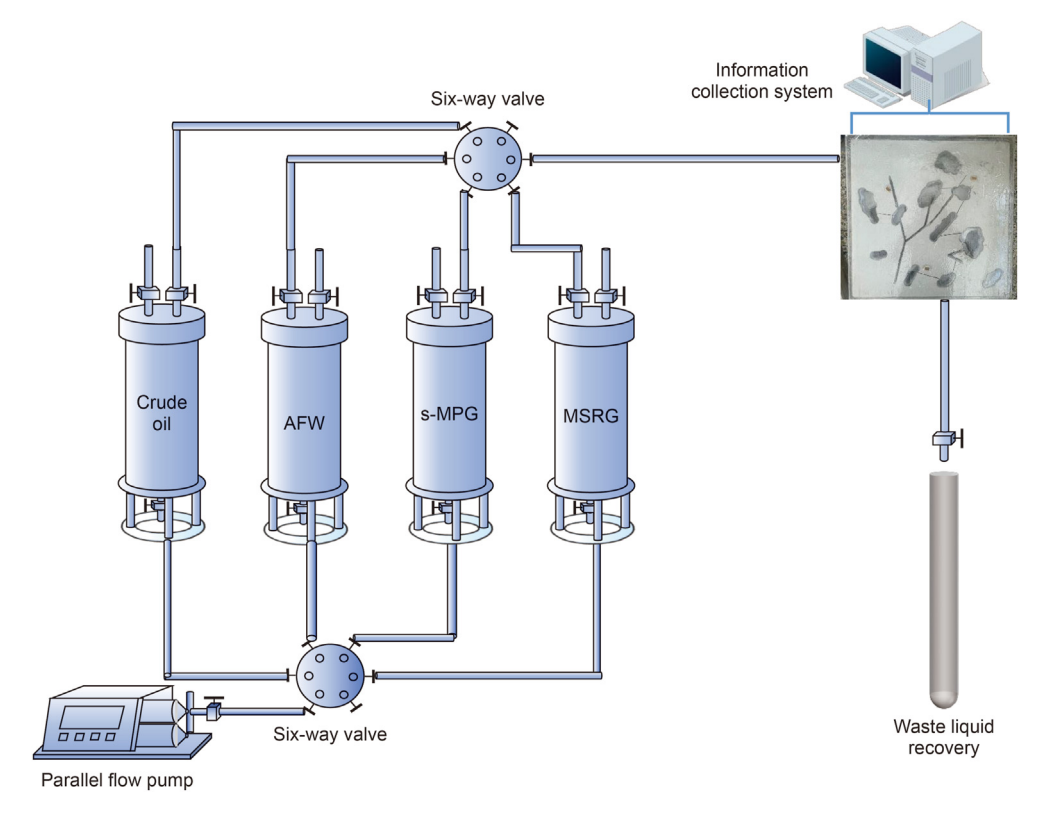


Fig. 2. Schematic diagram of the physical simulation experiment.

HP-WJ, weak acid accelerator HP-CJ, and CCH (cobalt chloride hexahydrate). HP-JL, HP-WJ, and HP-CJ are purchased from Haipeng Chemical Technology Co., Ltd., China. CCH is provided by Aladdin Biochemical Technology Co., Ltd., China. Briefly, 0.8 wt% AP-1 is fully dissolved in artificial formation water (AFW). Then, 0.5 wt% HP-JL, 0.3 wt% HP-WJ, and 0.5 wt% HP-CJ are added to the polymer solution in turn. After all agents are completely dissolved, 0.1 wt% CCH is added last. The ionic composition of AFW is shown in Table 1.

Modified starch resin gel (MSRG) is prepared using carboxymethyl modified starch MS-3, acrylamide (AM), N-methylidene bisacrylamide (MBA), BPO, ammonium persulfate (NH₄)₂S₂O₈, and Na₂SO₃. Briefly, 4.0 wt% MS-3 is fully dissolved in deionized water. Then, 4.0 wt% AM is added to the starch solution. Finally, 0.1 wt% MBA, 0.05 wt% (NH₄)₂S₂O₈, and 0.1 wt% Na₂SO₃ are added in turn.

2.2. Property characterization

The microstructure morphology of s-MPG and MSRG are characterized using EVOMA15/LS15 scanning electron microscope (SEM) (ZEISS, Germany). Besides, 80V infrared spectrum analyzer (Brooke, Germany) is used to analyze the functional groups of s-MPG and MSRG. Moreover, TG-DSC synchronous thermal analyzer (Mettler-Toledo, Switzerland) is used to characterize the temperature tolerance of bulk gel.

2.3. Dilution and compatibility properties of s-MPG and MSRG

The salinity of formation water in fractured-vuggy carbonate reservoir is generally higher than 20×10^4 mg/L and the energy of edge and bottom water is also very strong. Therefore, it is necessary to characterize the resistance to dilution and compatibility of s-MPG and MSRG. Briefly, the gel solution prepared with 24×10^4 mg/L AFW is poured into a beaker and gelatinized at high

temperature. And then, 10 g of bulk gel is taken out to be soaked in AFW. The interface between bulk gel and AFW can be obviously observed. The resistant dilution property of s-MPG and MSRG can be analyzed. Moreover, the synergistic effects of s-MPG and MSRG in AFW are also evaluated.

2.4. Physical simulation experiments

2.4.1. Design and manufacture of physical models

The similarity formula is shown in Table 2. Different types of fractured-vuggy models are designed while the key similarity coefficient is as close to 1 as possible. The model parameters are shown in Table 3.

The matrix permeability of physical model is less than 0.01 mD and the size of physical model is $20~\rm cm \times 20~\rm cm \times 4~\rm cm$. Reservoir types can be divided into fracture network, fragmentation zone, fractured-vuggy and karst-cave reservoirs. Fracture network reservoir develops micro-fractures in the form of multi-channel coning. Fragmentation zone reservoir develops main faults and secondary faults. Fractured-vuggy reservoir mainly develops fracture dissolution zone including hole edge cracks, bottom cracks and multi-fracture holes in parallel. Karst-cave reservoir exists in the form of isolated sinkholes. Various theoretical models and designed physical models are shown in Fig. 1.

2.4.2. Experimental processes

- (1) Vacuum the model for 6 h. Record the saturation volume of water and oil. Then, put these physical models in a high temperature oven for 5 days.
- (2) Water flooding is carried out at 5-10 mL/min until the water cut is more than 98%. Then, a certain amount of gel solution is injected into the physical model at 5 mL/min. In order to

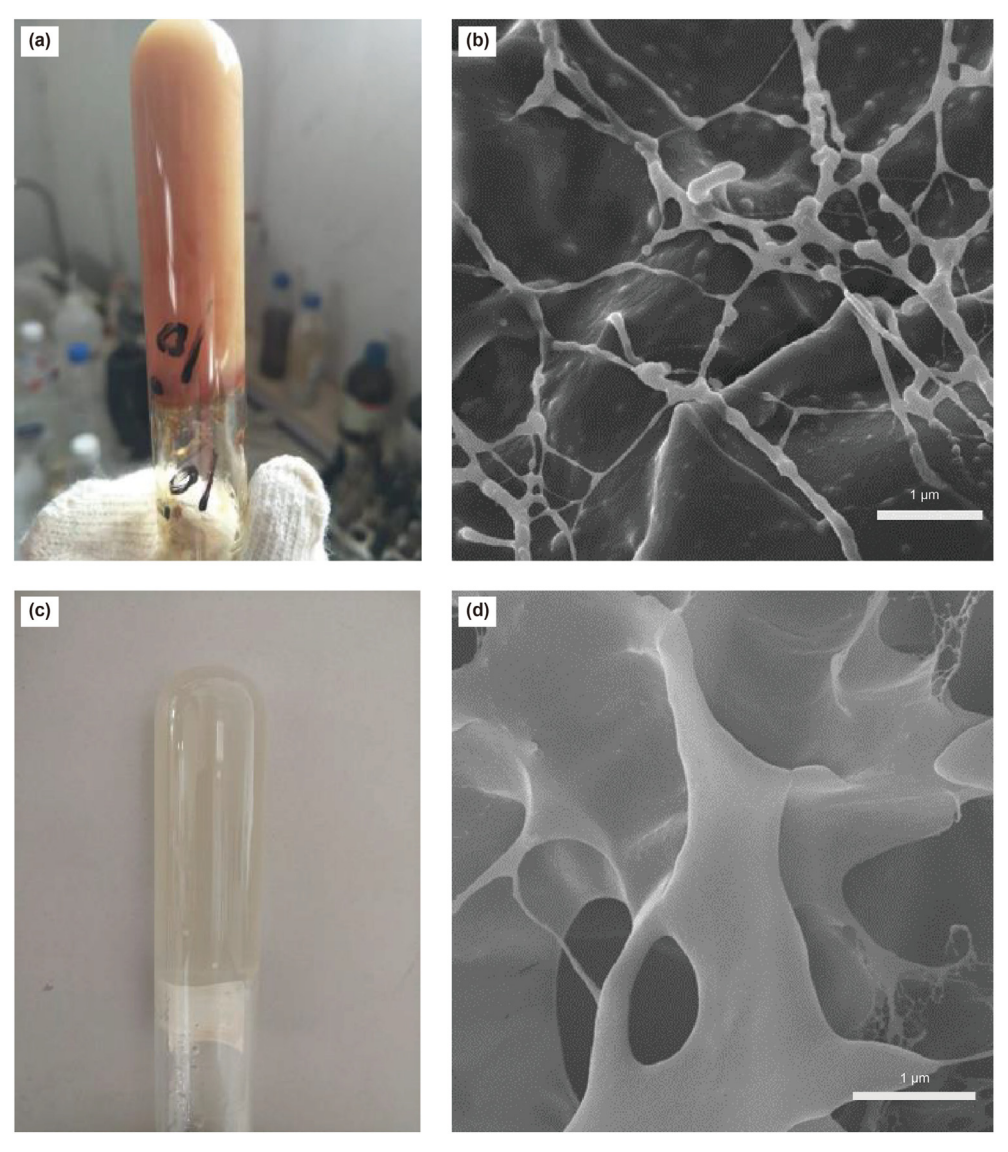


Fig. 3. Morphologies of s-MPG and MSRG bulk gel. (a) s-MPG; (b) SEM of s-MPG; (c) MSRG; (d) SEM of MSRG.

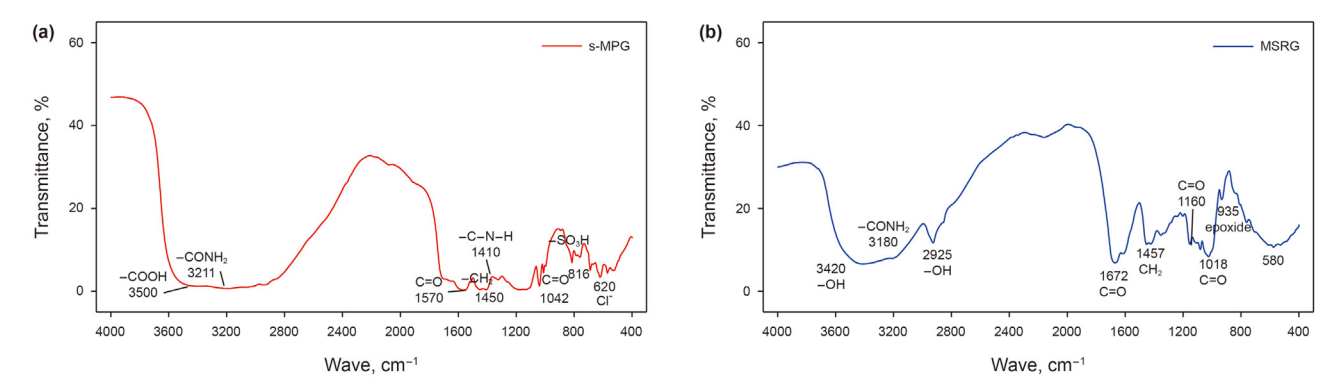


Fig. 4. FTIR results of bulk gel system. (a) s-MPG; (b) MSRG.

prevent bulk gel plugging the pipeline, a small amount of water is injected to clean the pipeline after finishing the gel solution injection. The physical model is aged at high temperature for 5 days until the gel solution is gelatinized.

(3) Secondary water flooding is injected at 5–10 mL/min after s-MPG or MSRG gelation. The secondary water flooding is stopped when the water cut is more than 98%. The schematic diagram of physical simulation experiment is shown in Fig. 2.

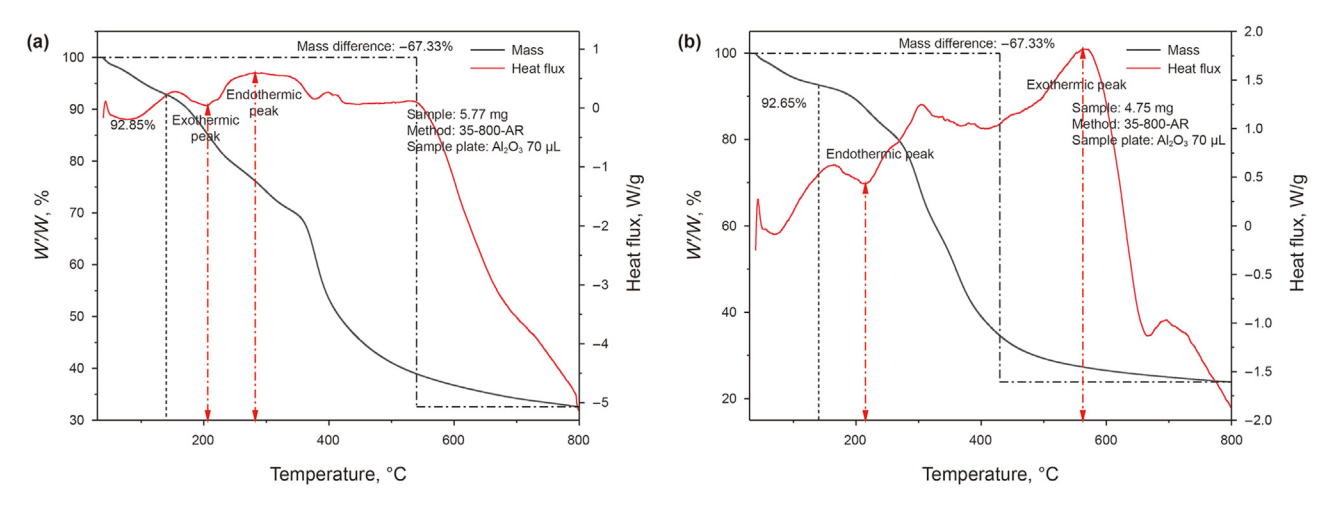


Fig. 5. TG-DSC results of bulk gel system. (a) s-MPG; (b) MSRG.

3. Results and discussion

3.1. Morphologies and physicochemical properties of s-MPG and MSRG

The synthesized s-MPG and MSRG bulk gel are shown in Fig. 3. The pre-processed solution is transferred into an oven and heated for 4 h at 140 °C to form s-MPG bulk gel as shown in Fig. 3(a), and the SEM microstructure of s-MPG is shown in Fig. 3(b). The MSRG bulk gel takes 3 h to gel at 140 °C, as shown in Fig. 3(c), and the SEM microstructure of MSRG is shown in Fig. 3(d). Based on the SEM images in Fig. 3(b) and (d), it can be determined that s-MPG and MSRG have a relatively stable 3D network dense structure after gelation, which can effectively form a stable gel respectively, and both of them have the basic morphology and performance suitable for profile control in-situ.

The functional groups of s-MPG and MSRG are characterized using FT-IR, as shown in Fig. 4 s-MPG gel (Fig. 4(a)) has a characteristic absorption peak at 3211 cm⁻¹, which is ascribed to the strong polymer amide groups (–CONH₂). Besides, an obvious absorption peak of free carboxyl group (–COOH) around 3500 cm⁻¹ occurs (Bode et al., 2013). Besides, high intensity absorption peak occurs at 1570 cm⁻¹ due to the C=O bond. The absorption peaks ranging from 1410 to 1450 cm⁻¹ are owing to the strong bending vibration of –CH₂ bond and –C–N–H– bond (del Prado et al., 2019; García Lodeiro et al., 2009). The high intensity absorption peak at 1042 cm⁻¹ is ascribed to C=O bond and the peak at 816 cm⁻¹ is due to the bending vibrational –SO₃H bond (Xia et al., 2021). In conclusion, s-MPG is mainly composed of amide group and sulfonate group, and also contains cross-linking agent and other small molecular stabilizers, which improves the salt resistance of s-MPG.

The FTIR diagram of MSRG is shown in Fig. 4(b). There is a strong absorbance peak in 3420 cm⁻¹ which is due to the –OH functional group. Besides, a high intensity absorption peak of –CONH₂ group occurs at 3180 cm⁻¹ and hydroxyl groups are associated in the vicinity of 2925 cm⁻¹ (Leng et al., 2023). In addition, the absorption peak at 1672 cm⁻¹ can be attributed to C=O bond in –COO–functional group. Moreover, the absorption peak at 1457 cm⁻¹ is owing to the –CH₂ bond in –CONH₂ group. The absorption peaks at 1160 and 1018 cm⁻¹ are ascribed to the C=O bond and the characteristic absorption band at 935 cm⁻¹ can be attributed to the epoxide compound (Deng et al., 2023; Liu et al., 2017). In conclusion, MSRG is not easy to be eroded by formation water due to the presence of epoxy compounds.

Fig. 5 shows the TG-DSC results of s-MPG and MSRG. Fig. 5(a)

indicates that the mass retention of s-MPG gel is 92.85% at 140 °C, showing excellent temperature resistance. Only adsorbed water can be evaporated at 140 °C and the main molecular chain cannot be degraded. When the temperature goes up to 355 °C, the hydrophilic groups are decomposed significantly and the thermal depolymerization reaction is intensified. The C=O bonds in amides and carboxyl groups are broken due to the increase of temperature, which leads to the cleavage of the main molecular chains. DSC results demonstrate that state of s-MPG changes gradually from glassy state to high elastic state at 104 °C. When the temperature reaches 150 °C, the curing enters exothermic state and the mass retention dramatically decreases. The molecular chain of the hydrophilic group is broken and the dehydration is intensified when the temperature is 355 °C. When the temperature comes to 540 °C, s-MPG is decomposed into gaseous state. Combined with the results of TG, the cleavage rate of the main molecular chains has begun to slow down after entering gaseous state, leading to the fact that s-MPG is dehydrated and degraded. In conclusion, s-MPG shows an excellent temperature resistance to adapt the ambient temperature of the target reservoir.

Fig. 5(b) shows the TG-DSC results of MSRG. The mass retention of MSRG gel is 92.65% at 140 $^{\circ}$ C, representing that MSRG gel has little weight loss below 140 °C. The phenomenon can be ascribed to the evaporation of adsorbed water and bound water (Firoozmand et al., 2007; Serrero et al., 2010). When the temperature increases to 200 °C, the thermal de-polymerization rate of MSRG accelerates. The thermal de-polymerization rate gradually slows down until the temperature exceeds 500 °C (Garai et al., 2006; Kim et al., 2023; Liu et al., 2017). Finally, the intermolecular loss is almost the same as s-MPG. DSC results indicate that state of MSRG changes gradually from glassy state to high elastic state at 76 °C. When the temperature reaches 160 °C, the curing enters the exothermic and the mass retention sharply decreases. Once the temperature goes up to 200 °C, the molecular chains of the hydrophilic groups are gradually broken and the dehydration is intensified (Worzakowska and Torres-Garcia, 2017). When the temperature exceeds 500 °C, MSRG is decomposed into gaseous. MSRG still meets the target reservoir's temperature of 140 °C even though MSRG enters the melting state earlier than s-MPG.

3.2. Properties of dilution resistance and compatibility

The dilution resistance of s-MPG and MSRG is evaluated because the edge and bottom water energy is very strong in fractured-vuggy carbonate reservoir. The contact state between high salinity AFW

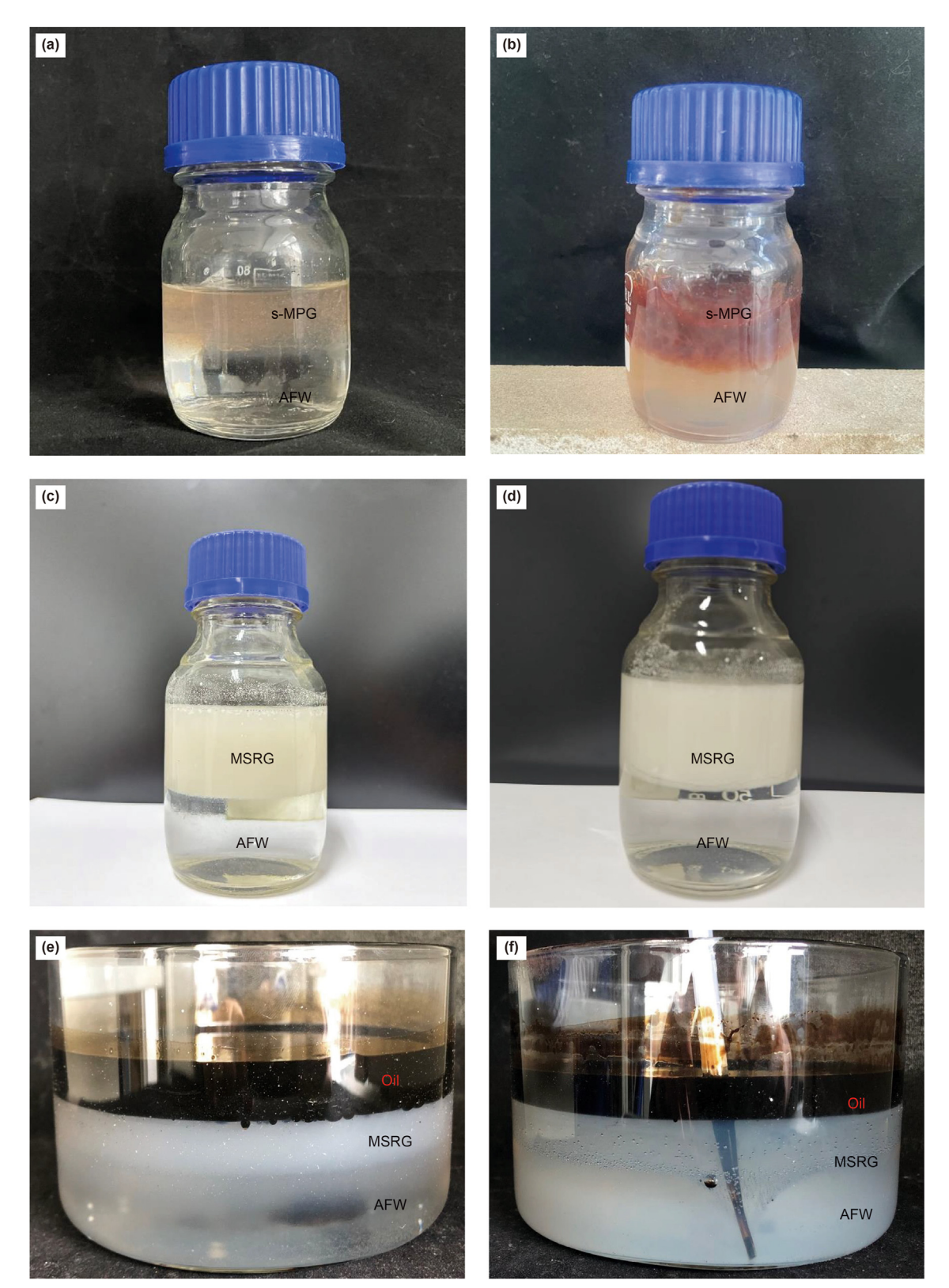


Fig. 6. Contact between gel system and AFW. (a) Before s-MPG aged; (b) After s-MPG aged; (c) Before MSRG aged; (d) After MSRG aged; (e) AFW-MSRG-oil before MSRG aged; (f) AFW-MSRG-oil after MSRG aged.

and s-MPG or MSRG gel solution in a vessel is prepared while the contact state among high salinity AFW, MSRG gel solution and crude oil is also prepared in a vessel. Finally, those vessels are put

into an oven with 140 $^{\circ}\text{C}.$ The experimental results are shown in Fig. 6.

As is shown in Fig. 6(a)–(d), s-MPG and MSRG contact with AFW

Table 4Anti-dilution ability of s-MPG and MSRG.

Gel	Bulk gel, g	Time, h	AFW, g	AFW after diluted, g	Poor quality, g	Dilution rate, %
s-MPG	10.18	3	103.57	104.48	0.91	8.94
	9.77	12	99.82	101.34	1.52	15.56
	11.45	24	102.16	104.30	2.14	18.69
MSRG	9.95	3	100.64	102.15	1.78	15.18
	9.87	12	101.25	103.23	2.61	20.06
	10.92	24	100.06	102.92	2.86	26.19



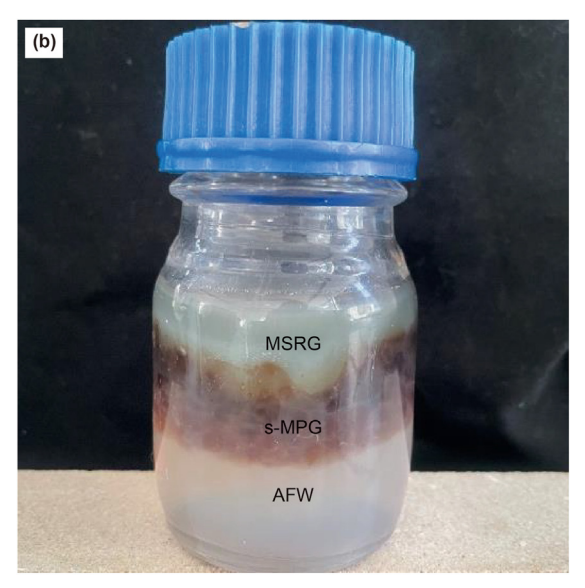


Fig. 7. Compatibility between s-MPG and MSRG in different order. (a) MSRG + s-MPG; (b) s-MPG + MSRG.

Table 5Experimental parameters of different physical simulation models.

Physical simulation model	Saturated volume, mL		Injection volume, PV		Injection rate, mL/min
	Crude oil	AFW	s-MPG	MSRG	
Fracture network	90	110	0.12 0.25	0.13	5
Fragmentation zone	60	70	0.11 0.23	0.12 /	5
Fractured-vuggy	140	160	0.14 0.28	0.14 /	5
Krast-cave	230	220	0.15 0.30	0.15 /	10

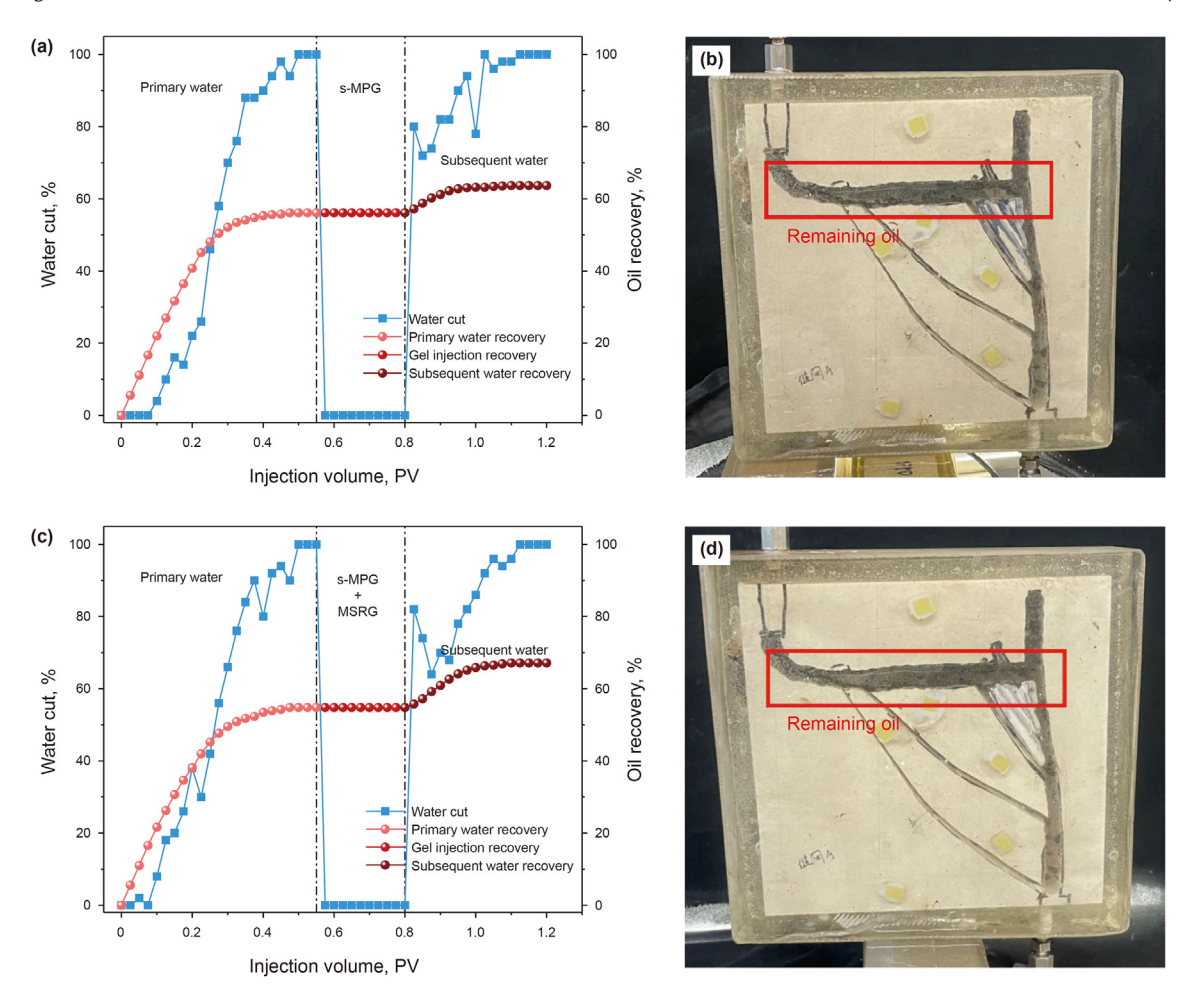
directly before aged. When s-MPG and MSRG are completely gelled, the cohesiveness of the gel separates it from AFW, respectively. Besides, Fig. 6(e) and (f) indicates that the addition of crude oil has no effect on the formation of gel because it keeps the contact state of AFW-MSRG gel solution-crude oil all the time. The poor quality method is used to further evaluate the dilution resistance of s-MPG and MSRG. Briefly, weigh 10 ± 2 g of s-MPG and MSRG, and then add them each to 100 g of AFW, respectively. The s-MPG mixture and MSRG mixture are placed into oven with $140~^{\circ}$ C for different time (3, 12, and 24 h) and then taken out for observation. Experimental results indicate that the dilution degree of s-MPG and MSRG are about 18.69% and 26.19% after 24~h, respectively, as shown in Table 4.

In the process of the transition from high viscosity liquid to viscoelastic colloid, dense cross-linking sites are formed among the molecular chains in the gel structure (Dong et al., 2023; Zhang et al., 2023). s-MPG and MSRG show stronger cohesion due to the

formation of 3D network structure causing by cross-linking association of functional groups. According to dilution rate from Table 4, the saturation degree of AFW in s-MPG structure is lower than that in MSRG structure. Therefore, s-MPG has the better ability in water control than that of MSRG.

Considering the dilution resistance and advantages of s-MPG and MSRG, an experiment on the compatibility of s-MPG and MSRG collaborative application is conducted. s-MPG and MSRG with same quality are used together to block AFW in an oven at 140 $^{\circ}\text{C}$, as shown in Fig. 7.

As can be seen from Fig. 7, s-MPG synergy with MSRG has obvious layering phenomenon. While MSRG synergy with s-MPG has no obvious layering phenomenon. The network structure of s-MPG is supported by polymer and phenolic cross-linking agent while metal ion compounds are regarded as stabilizers (He et al., 2023). Thus, s-MPG has smaller pore spaces, stronger cohesion and better intermolecular association. When s-MPG contacts with



 $\textbf{Fig. 8.} \ \, \textbf{Oil recovery and remaining oil distribution in fracture network model.} \ \, \textbf{(a, b)} \ \text{s-MPG;} \ \, \textbf{(c, d)} \ \text{s-MPG} + \text{MSRG.} \\$

AFW, both the hydrophobic association and salinity resistance are improved. However, the structure of MSRG is mainly supported by gelatinized starch and AM. During this reaction processes, the strength, stiffness and thermal stability of MSRG can be improved by the addition of hydrogen bond in carboxyl group (Li et al., 2021; Lv et al., 2023; Wan-En et al., 2023). When the pressure is applied to the upper and lower layers at the same time, the gel easily reaches the supersaturated state, resulting in a decrease in MSRG stability. Besides, the osmotic pressure of intermolecular in MSRG is weak, which also weakens the structural strength of MSRG. Research found that, s-MPG is consist of polymer, phenolic cross-linking agent, and other metal ion compounds. The polymer has significant pseudo-plasticity, thickening, shear reversibility, and thixotropic properties (Cancela et al., 2022; Du et al., 2021). The crosslinking groups of the polymer and the cross-linking agents react with each other by fusion, forming covalent, ionic or coordination bonds of different degrees, and forming a gel with a reticular structure at the ambient temperature, which improves the spatial positional resistance stability of the s-MPG gel system (Wu et al., 2022a). However, MSRG is consist of pre-gelatinized modified starch, AM, and agent containing reactive free radicals. Compared with s-MPG, it has good swelling, hydrophilic, and biodegradable properties. Meanwhile, the fundamental gelation mechanisms of s-MPG and MSRG are different, i.e., the gelation of both them will not interfere with each other. That is reason why s-MPG is more resistant to dilution than MSRG.

In addition, the experiments in Fig. 7 are conducted at in a

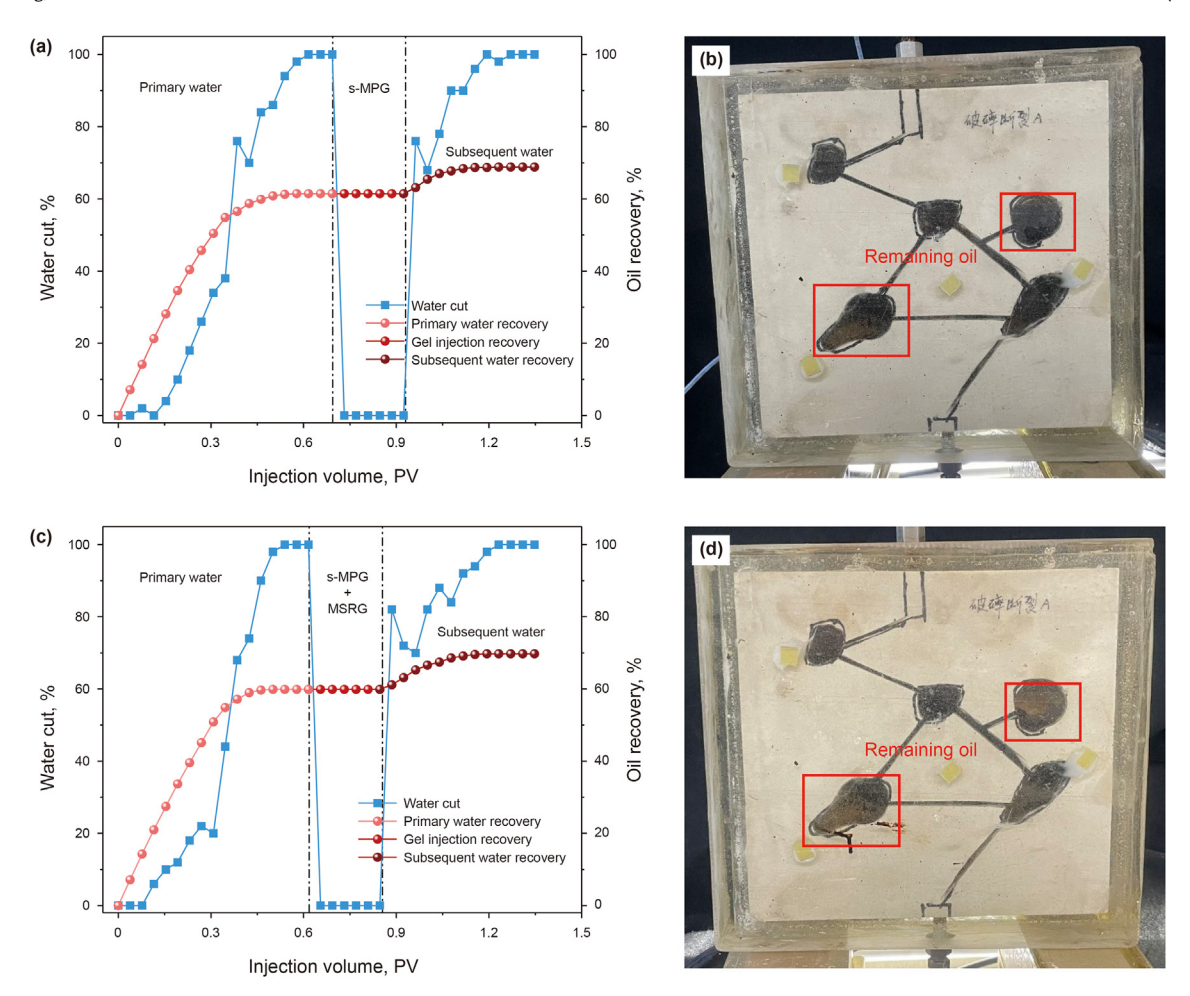
140 °C oven. According to the deeper the formation and the higher the temperature in the reservoir environment, the temperature gradient of a fractured-vuggy reservoir is about 2.2 °C/100 m. Hence, 140 °C represents about 6300 m underground in the reservoir. In conclusion, the synergy of s-MPG and MSRG can play a better in-depth profile control.

3.3. Physical simulation experiments

In this section, all of fractured-vuggy physical simulation models are saturated by crude oil and AFW, and then primary water flooding into model to displace crude oil until water cut exceeds 98%. Subsequently, s-MPG and MSRG are injected by constant velocity respectively with different volumes to each physical model. Then, secondary water flooding is conducted after each of gel system aged for several days. The experimental scheme is shown in Table 5. In order to verify the fact that s-MPG synergy with MSRG has better plugging efficiency than a single plugging agent, the same volume of s-MPG is also injected to each physical model.

3.3.1. Fracture network model experiment

Fig. 8(a) shows that the lowest water cut is 72% during secondary water flooding after s-MPG plugging and the oil recovery increases from 56.11% to 63.67%. Fig. 8(c) indicates that the lowest water cut is 64% during secondary water flooding after s-MPG synergy with MSRG plugging and the oil recovery increases from 54.78% to 67.11%.



 $\textbf{Fig. 9.} \ \, \textbf{Oil recovery and remaining oil distribution in fragmentation zone model.} \ \, \textbf{(a, b)} \ \text{s-MPG;} \ \, \textbf{(c, d)} \ \text{s-MPG} + \text{MSRG.} \\ \textbf{MSRG.} \ \, \textbf{(c, d)} \ \text{s-MPG} + \textbf{MSRG.} \\ \textbf{MSRG.} \ \, \textbf{(c, d)} \ \text{s-MPG} + \textbf{MSRG.} \\ \textbf{MSRG.} \ \, \textbf{(c, d)} \ \text{s-MPG} + \textbf{MSRG.} \\ \textbf{MSRG.} \ \, \textbf{(c, d)} \ \, \textbf{($

Fracture network reservoir has several characteristics: many fracture channels, strong bottom water energy, profile control and water plugging measures have high efficiency. After water plugging, the upper water channel is effectively suppressed and the remaining oil in the secondary channel is also mobilized. s-MPG has excellent thermal stability, dilution resistance, and erosion resistance in harsh conditions of high temperature and high salinity. On this basis, the addition of high-pressure-resistant and high-strength MSRG gel with condensation effect provides a better breakthrough pressure. Therefore, water plugging using s-MPG synergy with MSRG in fracture network reservoir can realize the water flow dominant channel plugging in the reservoir.

3.3.2. Fragmentation zone model experiment

Fig. 9(a) shows that the lowest water cut is 68% during secondary water flooding after s-MPG plugging and the oil recovery increases from 61.43% to 68.86%. Fig. 9(c) indicates that the lowest water cut is 70% during secondary water flooding after s-MPG synergy with MSRG plugging and the oil recovery increases from 59.86% to 69.71%.

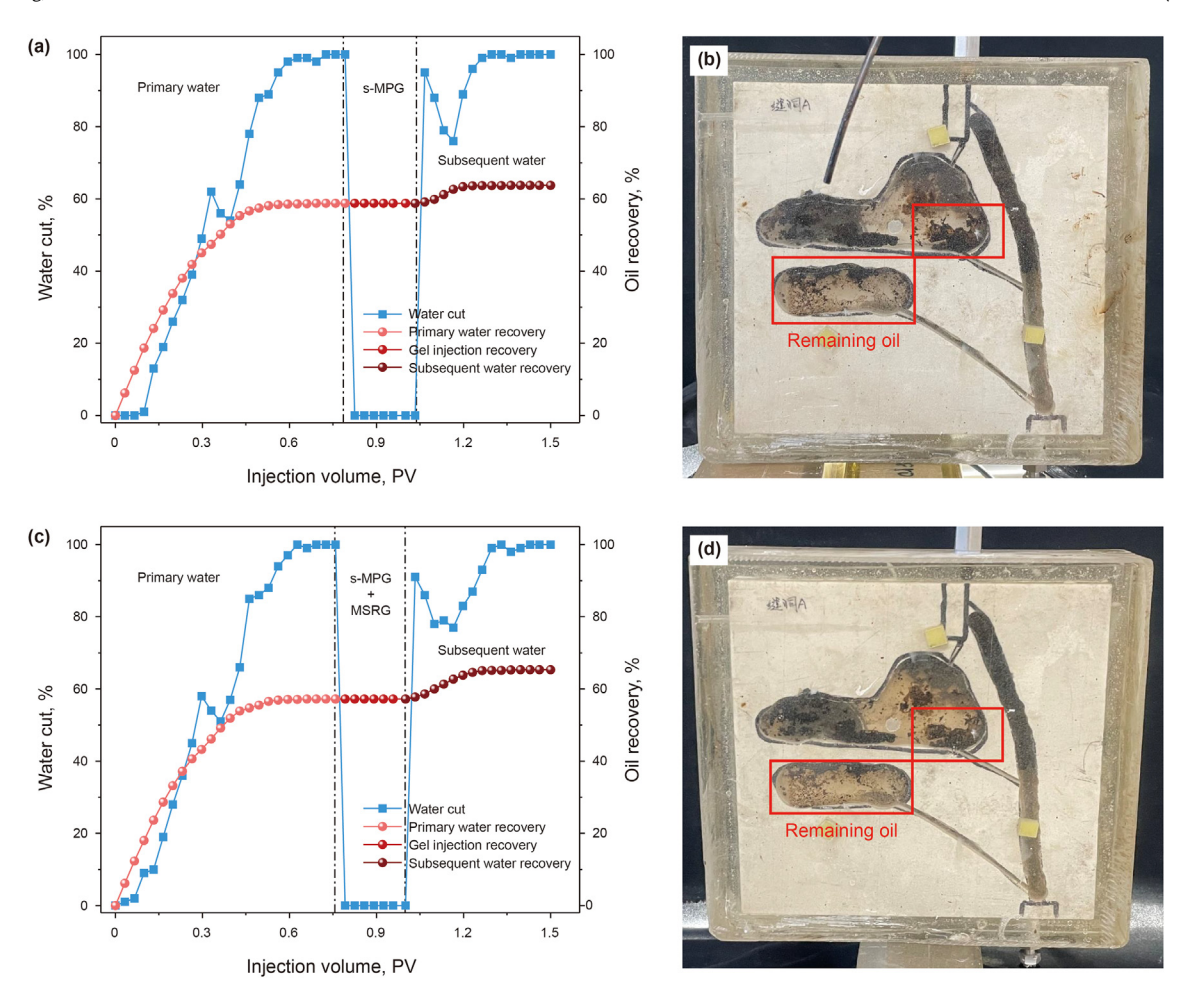
Fig. 9 demonstrates that the plugging effects of s-MPG is not as good as that of s-MPG synergy with MSRG, and the difference in oil recovery is about 2.5%. Fragmentation zone model shows several characteristics: wide distribution space, multi channels, complex fracture and irregular distribution. The water channeling in fragmentation zone model is single, and the scale of the main fracture is relatively large. The collaborative use of s-MPG and MSRG can

expand the swept volume, improve the plugging strength, plug part of the upper water channels and restrain the coning of bottom water. The s-MPG can be adsorbed on the rock surface to adjust the mobility ratio of water—oil in the formation due to its resistant to dilution, erosion and good fluidity. Therefore, the strength of subsequent MSRG can be guaranteed, leading to a fact that strong bottom water can be prevent. Therefore, more remaining oil distributed in the secondary channel in the fragmentation zone reservoir can be significantly mobilized using s-MPG synergy with MSRG.

3.3.3. Fractured-vuggy model experiment

Fig. 10(a) shows that the lowest water cut is 76% during secondary water flooding after s-MPG plugging and the oil recovery increases from 58.81% to 63.75%. Fig. 10(c) indicates that the lowest water cut is 78% during secondary water flooding after s-MPG synergy with MSRG plugging and the oil recovery increases from 57.19% to 65.31%.

Fig. 10 demonstrates that the plugging effects of s-MPG is not as good as that of s-MPG synergy with MSRG, and the difference in oil recovery is about 3%. Fractured-vuggy reservoir has several characteristics: large storage space and high permeability, fracture development and large bottom water energy. Therefore, the plugging agent should not only ensure the plugging strength, but also have an equivalent bulk breakthrough pressure. In fractured-vuggy reservoir, water plugging using s-MPG synergy with MSRG can plug water channeling to restrain the bottom water energy and



 $\textbf{Fig. 10.} \ \ \textbf{Oil recovery and remaining oil distribution in fractured-vuggy model.} \ \ \textbf{(a, b)} \ \ \text{s-MPG;} \ \ \textbf{(c, d)} \ \ \text{s-MPG} + \ \text{MSRG.}$

communicate secondary channels. The oil recovery can be also improved in the fractured-vuggy reservoir although the water control and oil increasing technology is more difficult to apply in fractured-vuggy reservoir than in fragmentation zone reservoir.

3.3.4. Karst-cave model experiment

Fig. 11(a) shows that the lowest water cut is 67% during secondary water flooding after s-MPG plugging and the oil recovery increases from 61.48% to 64.78%. Fig. 11(c) indicates that the lowest water cut is 59% during secondary water flooding after s-MPG synergy with MSRG plugging and the oil recovery increases from 59.91% to 65.14%.

Fig. 11 demonstrates that the plugging effects of s-MPG is not as good as that of s-MPG synergy with MSRG, and the difference in oil recovery is about 2%. The plugging effect in karst-cave reservoir is lower than that in other types of reservoirs, resulting in a lower oil recovery. Combined with the understanding of carbonate reservoir geological conditions, it is considered that the bottom water energy in karst-cave reservoir is larger than that in other types of reservoirs. Therefore, it is necessary to develop a kind of water plugging agent with high strength so that the gel can stay stable at the oil—water interface after gel solution diffusion and also the formed colloid wall is not too thin to be broken by strong bottom water energy. In addition, bulk gel cannot be gelatinized effectively due to the large volume of karst-cave reservoir space. Thereby, it is difficult to control the bottom water coning in karst-cave reservoir by

increasing the dosage and concentration of plugging agents.

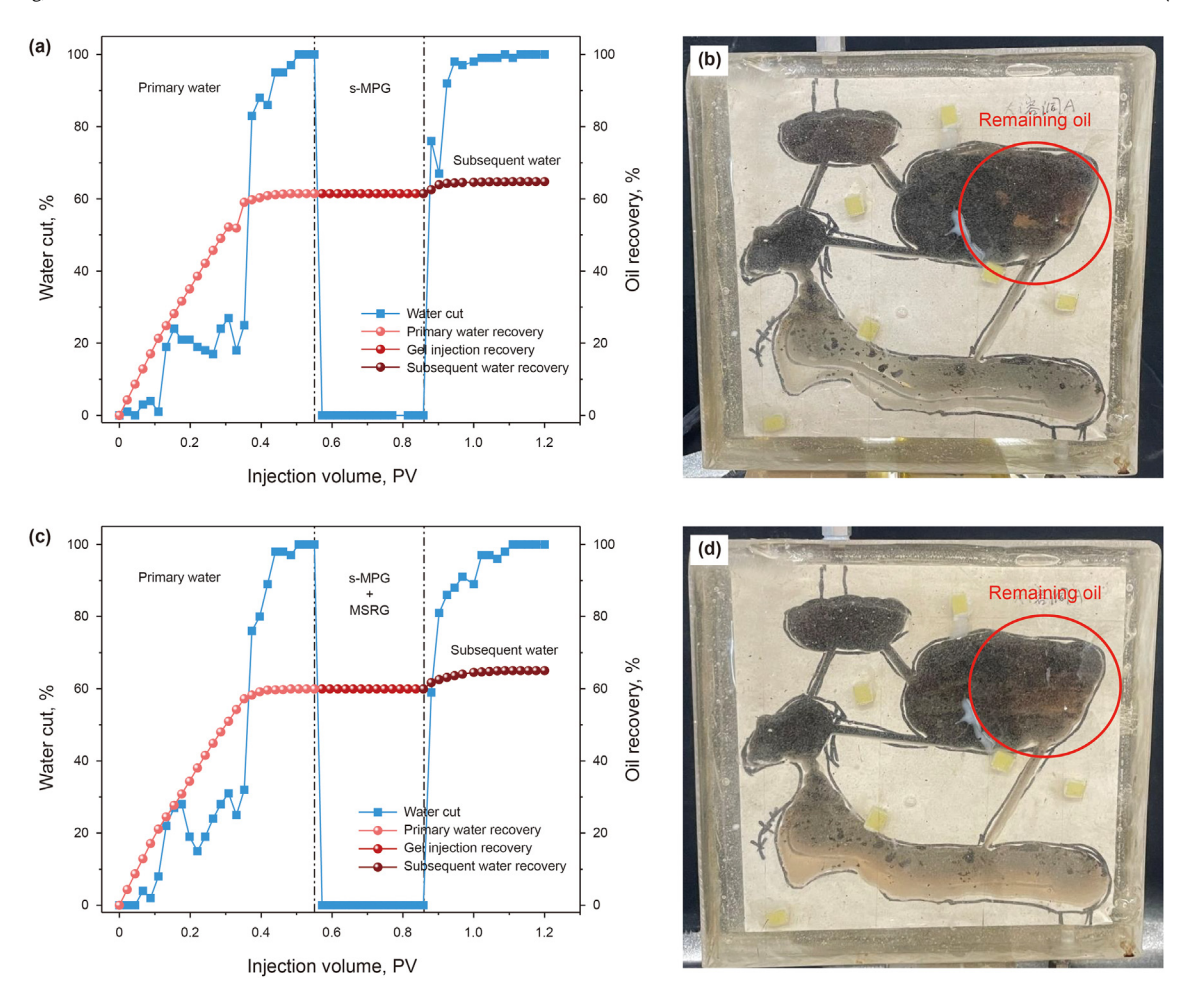
3.4. Adaptability analysis of water plugging in fractured-vuggy reservoir

Fractured-vuggy carbonate reservoir has large scale space and complex flow characteristics. Besides, bulk gel can expand in water and shrink in crude oil, and also can adsorb on the rock surface (Jin et al., 2021). Therefore, water plugging should meet the Navier—Stokes equation of hydrodynamic motion (Chen and Zhang, 2023), and the motion equation is as follows:

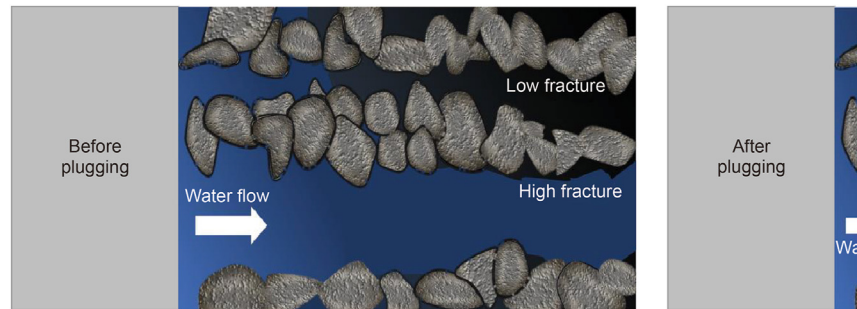
$$\frac{\partial a\rho}{\partial t} + \nabla \cdot \rho a \overrightarrow{v} = 0 \tag{1}$$

where α is the volume fraction of fluid, %; ρ is the density of fluid, kg/m³; \overrightarrow{v} is the velocity of fluid, m/s.

The gel, a continuous non-Newtonian fluid, can accumulate continuously during the migration process, leading to the formation-force and reaction-force with other fluids. According to Newton's second law, the forces of gel mainly include gravity, the interaction force between two kinds of gel solution and the interaction force between gel system and fluid (Ji et al., 2023). Especially, the drag force is produced between the two phases moving relative to each other. Therefore, the equation for describing the gel system motion can be expressed in Eq. (2):



 $\textbf{Fig. 11.} \ \, \textbf{Oil recovery and remaining oil distribution in Karst-cave model.} \, \textbf{(a, b)} \, \text{s-MPG;} \, \textbf{(c, d)} \, \text{s-MPG} + \text{MSRG.} \, \textbf{(c, d)} \, \text{s-MPG} + \textbf{(c, d)} \, \textbf{(c$



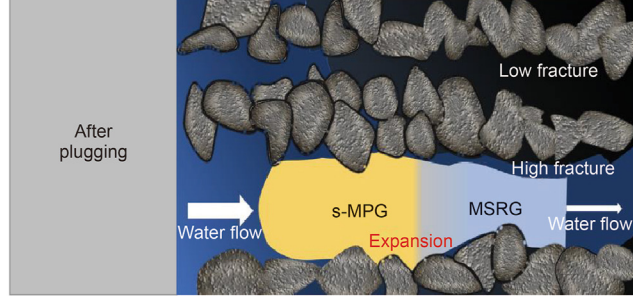


Fig. 12. Schematic diagram of towards in-depth profile control using s-MPG synergy with MSRG in fracture channel.

$$m\frac{\mathrm{d}v_{\mathrm{p}}}{\mathrm{d}t} = F_{\mathrm{D}} + F_{\mathrm{g}} + \sum F_{i} \tag{2}$$

where ν_P is the velocity of gel migration, m/s; F_D is the drag force of fluid, N; F_g is the force of gravity, N; F_i is the force between gel solutions, N.

The gel system meets the momentum conservation equation in the process of fluid motion, as shown in Eq. (3):

$$\frac{\partial(a\rho\nu)}{\partial t} + \nabla \cdot (\rho a\mu\nu) = -\nabla \rho + \nabla \cdot (\mu a\nabla \overrightarrow{\nu}) + \rho ag - \frac{\sum_{i=1}^{n} F_{D}}{V}$$
(3)

where g is the gravitational acceleration, m^2/s ; μ is the fluid viscosity, $kg/(m \cdot s)$; V is the unit volume, m^3 .

The reservoir with larger fracture width has higher permeability and flow capacity, leading to a fact that water phase has better fluidity than oil phase, so the water phase is mostly distributed in the high permeability zone with large fractures. During the process of water plugging, the migration ability of gel solution can be improved more easily in larger fractures. The gel solution enters the fractures to form high strength bulk gel, s-MPG synergy with MSRG for in-depth profile control in fractured-vuggy carbonate reservoirs. It can improve the probability of the gel system squeezing into the large fracture, and then control the dominant channel and then improve the plugging efficiency and long-term thermodynamic stability. Subsequently, secondary water flooding can expand

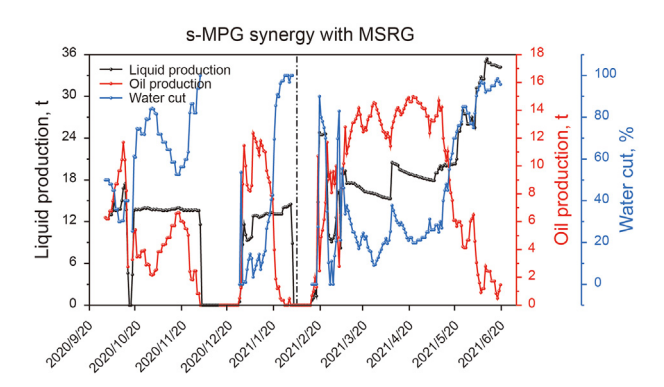


Fig. 13. Production curve of TKX34 well before and after s-MPG synergy with MSRG water plugging.

the swept volume and mobilize the secondary channels. The theoretical diagram is shown in Fig. 12.

4. Application in high temperature and ultra-high salinity reservoir in-situ

TKX34 well in a fractured-vuggy reservoir of Tahe Oilfield is a small-scale multi-cave well, each cave is connected by fractures, and the main oil reservoir is karst-cave. Because a strong bottom water cone is easily to form in TKX34 well, majority of plugging agents is washed by the bottom water for a long time and the breakthrough pressure reaches the upper limit prematurely, which leads to rapid failure. Towards in-depth profile control using 100 m³ s-MPG synergy with 100 m³ MSRG in TKX34 well. Viscoelastic fluid of s-MPG solution migrates intermittently to keep the wide spread range, which results in a good dilution resistance. Purely viscous fluid MSRG slowly accumulates in the dominant channel of water flow, forming a high-strength colloidal wall. Shutoff TKX34 wellhead at least 7 days after s-MPG and MSRG were injected, until the profile control agents aged and gelated completely. As expected, the water cut decreased from 100% to 30% and crude oil production increased by 14 t/d when the TKX34 well was open again. Finally, the stage cumulative crude oil production was 1142 t. The dynamic production curve is shown in Fig. 13.

5. Conclusions

- (1) s-MPG is based on the copolymer of sulfonate group and amide group as main chain, high temperature stabilizer was be added to improve molecular chains and maintain stability, steric hindrance will increase based on hydroxymethylation reactions and intermolecular interactions, the 3D structure of s-MPG will be denser.
- (2) MSRG uses modified starch and AM graft polymerization to improve molecular chain stability. The dehydration and condensation effects can improve the molecular efficiency of bound water. Peroxide initiators can improve the mutual association between molecular chains and stabilizes the connection of chemical bonds.
- (3) At 140 °C, the quality retention rate of s-MPG is 92.85% and MSRG is 92.65%. In 24×10^4 mg/L high salinity water, the dilution rate of s-MPG is about 18.69% and MSRG is about 26.69%. s-MPG synergy with MSRG in fractured-vuggy carbonate reservoirs has good compatibility and adaptability due to a fact that anti-dilution s-MPG can separate bottom water and high strength MSRG can separate oil layer.

- (4) Compared with single gel plugging fractured-vuggy reservoirs, the s-MPG synergy with MSRG plugging is better for enhanced oil recovery. The oil recovery in fracture network reservoir is increased by 12%, the oil recovery in fragmentation zone reservoir is increased by 10%, and the oil recovery in fractured-vuggy reservoir and karst-cave reservoir are increased by 8% and 5%, respectively.
- (5) s-MPG synergy with MSRG can better stabilize the gel structure to block the fracture channel, weaken the bottom water energy erosion, adjust the oil-water flow space, and inhibit water content in fractured-vuggy carbonate reservoirs. Production data of Well TKX34 shows that, the water cut is reduced from 100% to 30%, and the cumulative oil production increases to 1142 t.

CRediT authorship contribution statement

Wei-Peng Wu: Writing — review & editing, Writing — original draft, Visualization, Validation, Methodology, Investigation, Formal analysis, Data curation, Conceptualization. Min Yang: Writing — review & editing, Methodology, Investigation. Dong-Chen Ma: Writing — review & editing, Writing — original draft, Visualization. Ji-Rui Hou: Writing — review & editing, Investigation, Data curation. Tuo Liang: Writing — review & editing, Writing — original draft, Visualization, Validation, Supervision. Ming Qu: Writing — review & editing, Supervision, Investigation. Tao Tan: Writing — original draft, Data curation. Biao Yang: Writing — original draft. Guo-Rui Ma: Visualization, Data curation.

Declaration of competing interest

The authors declare that they have no known competing financial interests or personal relationships that could have appeared to influence the work reported in this paper.

Acknowledgment

The authors gratefully appreciate the financial support of Sinopec Northwest Oilfield Company, Xinjiang Urumqi (Grant No. K[202336).

References

Bode, S., Linda, Z., Schacher, F.H., et al., 2013. Self-healing polymer coatings based on crosslinked metallosupramolecular copolymers. Adv. Mater. 25 (11), 1634–1638. https://doi.org/10.1002/adma.201203865.

Cancela, B.R., Palermo, L.C.M., de Oliveira, P.F., et al., 2022. Rheological study of polymeric fluids based on HPAM and fillers for application in EOR. Fuel 330, 125647. https://doi.org/10.1016/j.fuel.2022.125647.

Chen, Q., Zhang, Q., 2023. Energy equality of the weak solutions to Navier—Stokes equations in the multiplier spaces. Appl. Math. Lett. 146, 108814. https:// doi.org/10.1016/j.aml.2023.108814.

del Prado, A., Hohl, D.K., Balog, S., et al., 2019. Plant oil-based supramolecular polymer networks and composites for debonding-on-demand adhesives. ACS Appl. Polym. Mater. 1 (6), 1399–1409. https://doi.org/10.1021/acsapm.9b00175.

Deng, L., Li, Y., Zhong, G., et al., 2023. Effects of starch addition on kgm sol's pasting, rheological properties, and gel texture. ACS Omega 8 (37), 33299–33309. https://doi.org/10.1021/acsomega.3c02265.

Dong, S., He, L., Li, L., Wu, Y., et al., 2023. Investigation of polyvinyl alcohol—phenolic aldehyde—polyacrylamide gel for the application in saline oil reservoirs for profile modification. Energy Fuels 37 (18), 13710—13720. https://doi.org/10.1021/acs.energyfuels.3c02178.

Du, L., Xiao, Y.Y., Jiang, Z.C., et al., 2023. Towards in-depth profile control using dispersed particle gels (DPGs). Fuel 354, 129419. https://doi.org/10.1016/ j.fuel.2023.129419.

Du, Y., Zhu, Y.W., Ji, Y.F., et al., 2021. Effect of salt-resistant monomers on viscosity of modified polymers based on the hydrolyzed poly-acrylamide (HPAM): A molecular dynamics study. J. Mol. Liq. 325, 115161. https://doi.org/10.1016/ i.mollig.2020.115161.

Emad, W., Salih, A., Kurda, R., 2021. Stress-stain behavior, elastic modulus, and

toughness of the soilcrete modified with powder polymers. Construct. Build. Mater. 295, 123621. https://doi.org/10.1016/j.conbuildmat.2021.123621.

- Firoozmand, H., Murray, B.S., Dickinson, E., 2007. Fractal-type particle gel formed from gelatin plus starch solution. Langmuir 23 (8), 4646–4650. https://doi.org/10.1021/la063664g.
- Garai, A., Kuila, B.K., Nandi, A.K., 2006. Montmorillonite clay nanocomposites of sulfonic acid doped thermoreversible polyaniline gel: Physical and mechanical properties. Macromolecules 39 (16), 5410–5418. https://doi.org/10.1021/ ma060636w.
- García Lodeiro, I., Macphee, D.E., Palomo, A., et al., 2009. Effect of alkalis on fresh C–S–H gels. FTIR analysis. Cement Concr. Res. 39 (3), 147–153. https://doi.org/10.1016/j.cemconres.2009.01.003.
- He, Y., Dong, K.Y., Guo, Y.D., et al., 2023. Preparation and properties of the cross-linked poly(L-lactide) with high crystallinity and high gel content. Polymer 287, 126441. https://doi.org/10.1016/j.polymer.2023.126441.
- Ji, X., Gabbard, J., van Rees, W.M., 2023. A sharp immersed method for 2D flow-body interactions using the vorticity-velocity Navier-Stokes equations. J. Comput. Phys. 494, 112513. https://doi.org/10.1016/j.jcp.2023.112513.
- Jiao, F.Z., 2019. Practice and knowledge of volumetric development of deep fractured-vuggy carbonate reservoirs in Tarim Basin, NW China. Petrol. Explor. Dev. 46 (3), 576–582. https://doi.org/10.1016/S1876-3804(19)60037-6.
- Jin, F.Y., Jiang, T.T., Varfolomeev, M.A., et al., 2021. Novel preformed gel particles with controllable density and its implications for EOR in fractured-vuggy carbonated reservoirs. J. Petrol. Sci. Eng. 205, 108903. https://doi.org/10.1016/ i.petrol.2021.108903.
- Jothi Arunachalam, S., Saravanan, R., 2023. Study on filler reinforcement in polymer matrix composites—A review. Mater. Today: Proc. https://doi.org/10.1016/ i.matpr.2023.06.102.
- Khoshkar, P.A., Fatemi, M., Ghazanfari, M.H., 2020. Static and dynamic evaluation of the effect of nanomaterials on the performance of a novel synthesized PPG for water shut-off and improved oil recovery in fractured reservoirs. J. Petrol. Sci. Eng. 189, 107019. https://doi.org/10.1016/j.petrol.2020.107019.
- Kim, S.K., Jung, H.W., Son, D., et al., 2023. In situ reactive compatibilization of thermoplastic starch/poly(butylene adipate-co-terephthalate) blends with robust water resistance performance. ACS Appl. Polym. Mater. 5 (7), 5445–5453. https://doi.org/10.1021/acsapm.3c00774.Leng, G.Y., Yan, W., Li, F.L., et al., 2023. Improved oil recovery in sandstone reservoirs
- Leng, G.Y., Yan, W., Li, F.L., et al., 2023. Improved oil recovery in sandstone reservoirs with deep profile control technology: a comparative study between modified starch gel and polymer gel. Geoenergy Science and Engineering 226, 211697. https://doi.org/10.1016/j.geoen.2023.211697.
- Li, H.B., Wang, G.W., Li, Y.H., et al., 2023. Fault-Karst systems in the deep ordovician carbonate reservoirs in the yingshan formation of Tahe Oilfield tarim basin, China. Geoenergy Science and Engineering 231 (Part A), 212338. https://doi.org/10.1016/j.geoen.2023.212338.
- Li, Z.Y., Wang, Y.F., He, H., et al., 2021. Insights into the effects of salinity on the transport behavior of polymer-enhanced branched-preformed particle gel suspension in porous media. Energy Fuels 35 (2), 1104–1112. https://doi.org/ 10.1021/acs.energyfuels.0c03159.
- Liu, J.W., Li, C., Sun, C., et al., 2017. Insights into the silanization processes of silica with and without acid—base additives via TG-FTIR and kinetic simulation. Ind. Eng. Chem. Res. 56 (18), 5164—5173. https://doi.org/10.1021/acs.iecr.6b04866.
- Lu, S.Y., Liu, Q.F., Li, P.L., et al., 2024. Preparation and enhancement mechanisms of a novel modified nanographite hybrid polymer gel for profile control in deep reservoirs. Colloids Surf. A Physicochem. Eng. Asp. 681, 132774. https://doi.org/ 10.1016/j.colsurfa.2023.132774.
- Lv, D.F., Li, J.M., Bo, Q.W., et al., 2023. A novel profile control agent in high-temperature and high-salinity reservoirs: dispersed particle gel prepared from modified nanographite-strengthened bulk gel. Energy Fuels 37 (24),

- 19487-19498. https://doi.org/10.1021/acs.energyfuels.3c03478.
- Parikh, H.H., Chokshi, S., Chaudhary, V., et al., 2023. Flexural response of 3D printed wood dust reinforced polymer composite. Mater. Today: Proc. https://doi.org/ 10.1016/j.matpr.2023.06.375.
- Qu, M., Hou, J.R., Qi, P.P., et al., 2018. Experimental study of fluid behaviors from water and nitrogen floods on a 3-D visual fractured-vuggy model. J. Petrol. Sci. Eng. 166, 871–879. https://doi.org/10.1016/j.petrol.2018.03.007.
- Salunkhe, B., Schuman, T., Al Brahim, A., et al., 2021. Ultra-high temperature resistant preformed particle gels for enhanced oil recovery. Chem. Eng. J. 426, 130712. https://doi.org/10.1016/j.cej.2021.130712.
- Serrero, A., Trombotto, S., Cassagnau, P., et al., 2010. Polysaccharide gels based on chitosan and modified starch: structural characterization and linear viscoelastic behavior. Biomacromolecules 11 (6), 1534–1543. https://doi.org/10.1021/ bm1001813
- Wan-En, O., Yun-Ming, L., Cheng-Yong, H., et al., 2023. Acid-resistance of one-part geopolymers: sodium aluminate and carbonate as alternative activators to conventional sodium metasilicate and hydroxide. Construct. Build. Mater. 404, 133264. https://doi.org/10.1016/j.conbuildmat.2023.133264.
- Wang, J., Qi, X.S., Liu, H.Q., et al., 2022a. Mechanisms of remaining oil formation by water flooding and enhanced oil recovery by reversing water injection in fractured-vuggy reservoirs. Petrol. Explor. Dev. 49 (5), 1110–1125. https://doi.org/10.1016/S1876-3804(22)60336-7.
- Wang, T.F., Wang, L.L., Wang, J.X., et al., 2022b. In-situ emulsification synergistic self-profile control system on heavy oil reservoir development: prescription construction and EOR mechanism investigation. J. Petrol. Sci. Eng. 219, 111069. https://doi.org/10.1016/j.petrol.2022.111069.
- Wen, Y.C., Hou, J.R., Xiao, L.X., et al., 2023. Utilization mechanism of foam flooding and distribution situation of residual oil in fractured-vuggy carbonate reservoirs. Petrol. Sci. 20 (3), 1620–1639. https://doi.org/10.1016/j.petsci.2022.11.020.
- Worzakowska, M., Torres-Garcia, E., 2017. The effect of the grafting percentage of starch-g-poly(phenyl acrylate) copolymers on their pyrolysis and kinetics studied by the TG/DSC/FTIR/QMS-coupled method. Polym. Degrad. Stabil. 139, 67–75. https://doi.org/10.1016/j.polymdegradstab.2017.03.019.
- Wu, W.P., Hou, J.R., Qu, M., et al., 2022a. A novel polymer gel with high-temperature and high-salinity resistance for conformance control in carbonate reservoirs.
 Petrol. Sci. 19 (6), 3159–3170. https://doi.org/10.1016/j.petsci.2022.05.003.
 Wu, W.P., Hou, J.R., Qu, M., et al., 2022b. Application of phenolic resin crosslinked
- Wu, W.P., Hou, J.R., Qu, M., et al., 2022b. Application of phenolic resin crosslinked polymer gel in fractured-vuggy carbonate reservoir with high temperature and high salinity. In: International Petroleum Technology Conference. https:// doi.org/10.2523/IPTC-22440-MS.
- Xia, X.M., Wang, X., Han, X.K., et al., 2021. Construction of self-assembled nanogel as mulitenzyme mimics for bioresponsive tandem-catalysis imaging. Sci. China Mater. 64 (12), 3079–3086. https://doi.org/10.1007/s40843-021-1697-x (In Chinese).
- Xu, B.Z., Lv, D.F., Zhou, D.Y., et al., 2024. Potential application of wet-phase modified expandable graphite particles as a novel in-depth profile control agent in carbonate reservoirs. Petrol. Sci. https://doi.org/10.1016/j.petsci.2024.07.008.
- Yang, W., Zhang, D., 2022. Experimental study on multiphase flow in 3D-printed heterogeneous, filled vugs. J. Petrol. Sci. Eng. 208 (Part C), 109497. https:// doi.org/10.1016/j.petrol.2021.109497.
- Zhang, G.T., Cai, X.X., Li, C., et al., 2023. Construction of alkaline gel polymer electrolytes with a double cross-linked network for flexible zinc—air batteries. ACS Appl. Polym. Mater. 5 (5), 3622—3631. https://doi.org/10.1021/acsapm.3c00270.
- Zhao, Y.L., Lu, G., Zhang, L.H., et al., 2020. Physical simulation of waterflooding development in large-scale fractured-vuggy reservoir considering filling characteristics. J. Petrol. Sci. Eng. 191, 107328. https://doi.org/10.1016/ j.petrol.2020.107328.